ACS APPLIED MATERIALS & INTERFACES

Research Article

www.acsami.org

# Synthesis of Photoluminescent Au ND−PNIPAM Hybrid Microgel for the Detection of $Hg^{2+}$

Li-Yi Chen,[†] Chung-Mao Ou,[†] Wei-Yu Chen,[†] Chih-Ching Huang,[‡,§] and Huan-Tsung Chang*[,†]

[†]Department of Chemistry, National Taiwan University, Taipei 10617, Taiwan

[‡]Institute of Bioscience and Biotechnology and [§]Center of Excellence for Marine Bioenvironment and Biotechnology, National Taiwan Ocean University, Keelung 20224, Taiwan

Supporting Information

**ABSTRACT:** Poly(*N*-isopropylacrylamide) microgels (PNIPAM MGs) incorporated with photoluminescent gold nanodots (Au NDs) have been prepared and employed for the detection of mercury ions ($Hg^{2+}$). Each of the PNIPAM MGs (hydrodynamic diameter 615 ± 15 nm) contains several Au NDs (diameter 1.8 ± 0.2 nm) in the Au ND−PNIPAM MGs. Like Au NDs, Au ND−PNIPAM MGs exhibit an absorption band at 375 nm that is assigned for ligand to metal charge transfer mixed with metal centered (ds/dp) states and photoluminescence at 520 nm originated from Au ND/polynuclear gold(I)−thiolate (core/shell) complexes. Purification of Au ND−PNIPAM MGs relative to Au NDs is much easier through a simple centrifugation/wash process. On the basis of $Hg^{2+}$-induced photoluminescence quenching due to the formation of Au−Hg amalgam and formation of Au ND−PNIPAM MGs aggregates, the signal response of Au ND−PNIPAM MGs against $Hg^{2+}$ concentration is linear over a range from 2 to 20 nM ($r$ = 0.9945). This selective approach provides limits of detection for $Hg^{2+}$ (at a signal-to-noise ratio of 3) of 1.9 and 1.7 nM in phosphate buffer solutions (5 mM, pH 7.0) with and without containing 500 mM NaCl, respectively. This selective and sensitive Au ND−PNIPAM MG probe has been applied to the determination of the concentration of Hg in a representative fish sample, showing its practical potential for monitoring of Hg levels in complicated biological and environmental samples.

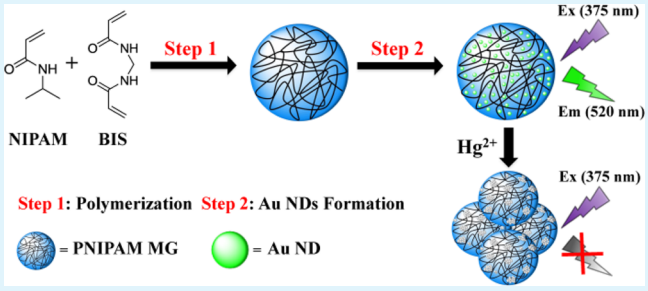


**KEYWORDS:** *poly(N-isopropylacrylamide), microgel, photoluminescent, gold nanodots, mercury detection*

## INTRODUCTION

Detection of toxic mercury (Hg) in aquatic ecosystems is important because it can have severe effects on human health and the environment.[1] The U.S. Environmental Protection Agency (EPA) has set the maximum allowable levels of Hg in drinking water at 10 nM (2.0 ppb). Inductively coupled plasma mass spectrometry (ICP−MS) is popular for the monitoring of $Hg^{2+}$ level in environmental samples, mainly because of its advantages of great sensitivity, a wide dynamic range, and low matrix interference. The system is, however, quite expensive and uses large amount of expensive argon gas. Thus sensitive, selective, simple, and cost-effective detection approaches are still demanded for the detection of trace amounts of $Hg^{2+}$ in complicated environmental samples.

Having high molar absorptivity and stability, gold nanoparticles (Au NPs) capped with recognition elements such as 3-mercaptopropionic acid have been used for the detection of $Hg^{2+}$.[2−4] These detection systems are based on the changes in the absorption (color) due to analyte-induced aggregation of Au NPs. By taking the advantage of high quenching efficiency of Au NPs, Au NP-adsorbed rhodamine B in the presence of 1.0 mM 2,6-pyridinedicarboxylic acid allows the detection of $Hg^{2+}$ down to 10 nM.[5] Alternatively, photoluminescent Au nanodots (NDs) with large Stokes shifts, long lifetimes, and high water solubility have become interesting sensing materials for the detection of $Hg^{2+}$,[6−13] based on the analyte-induced photoluminescence (PL) quenching. In addition, photoluminescent oligonucleotide-, dihydrolipoic acid-, and protein-stabilized Ag nanoclusters (NCs) have become attractive for the sensitive detection of $Hg^{2+}$.[14−16]

To further improve the selectivity, aptamer-functionalized Au NPs (Apt−Au NPs) have been applied for the detection of $Hg^{2+}$.[17−19] Free aptamers in conjunction with fluorophores and aptamers covalently conjugated with donors and acceptors are also popular probes for the detection of $Hg^{2+}$ through the analyte-induced DNA conformational changes and thus fluorescence changes.[20,21] In addition, highly sensitive electrochemical sensing systems using $Hg^{2+}$-specific aptamer and Au NPs through signal amplification have been exploited for the detection of $Hg^{2+}$ ions in aqueous solution.[22,23] The sensing systems are sensitive and selective, but aptamers are expensive relative to most organic recognition elements. Alternatively, many chemical recognition elements have been used for

Received: February 19, 2013
Accepted: April 25, 2013
Published: April 25, 2013

  

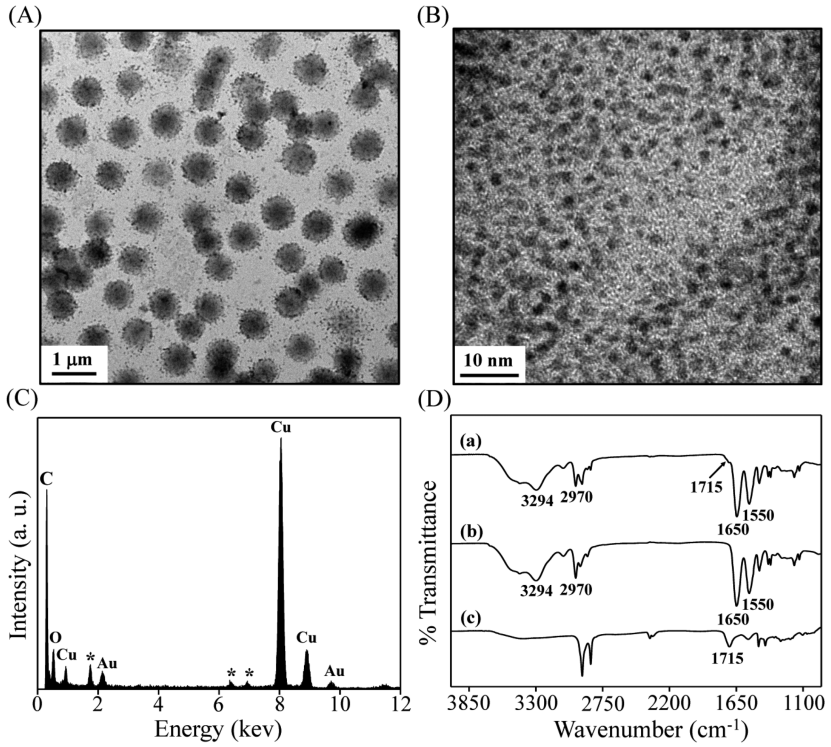


**Figure 1.** (A) TEM image, (B) high-resolution TEM image (C) EDX spectrum, and (D) FTIR spectrum of the Au ND−PNIPAM MGs. (C) * is the background from the system. (D) (a) Au ND−PNIPAM MGs, (b) PNIPAM MGs, and (c) 11-MUA−Au NDs. The band at 1715 $cm^{-1}$ was assigned for the carboxylate group from 11-MUA in Au ND−PNIPAM MGs, as marked in the arrow.

sensitive and selective detection of $Hg^{2+}$ ions through analyte-induced changes in their fluorescence and absorption.[24−26]

One main concern of the developed sensing systems for $Hg^{2+}$ is that their selectivity and sensitivity are highly dependent on solution pH and ionic strength, limiting their application to simple sample systems. To overcome this limitation, we prepared Au NDs inside poly(*N*-isopropylacrylamide) (PNIPAM) microgels (MGs). Various compositions, shapes, and sizes of hybrid MGs exhibiting temperature sensitive microstructures have been prepared.[27−31] The Au ND−PNIPAM MGs relative to the Au NDs were more stable against salt and were purified more easily by conducting a simple centrifugation/wash process. We carefully investigated important factors such as solution pH and salt concentrations (e.g., NaCl) to optimize the sensitivity and selectivity for the detection of $Hg^{2+}$. The Au ND−PNIPAM MGs were applied to the detection of $Hg^{2+}$ in aqueous solutions containing NaCl up to 500 mM and in a fish sample through PL quenching.

## MATERIALS AND METHODS

**Chemicals.** Hydrogen tetrachloroaurate(III) trihydrate ($HAuCl_4{\cdot}3H_2O$) and *N*-isopropylacrylamide (NIPAM) were obtained from Acros (Geel, Belgium, USA). Mercury chloride, 11-mercaptoundecanoic acid (11-MUA), tetra(hydroxymethyl)phosphonium chloride (THPC), and potassium peroxodisulfate (KPS) were purchased from Aldrich (Milwaukee, WI, USA). *N*,*N*′-Methylenebisacrylamide (BIS) was purchased from Bio-Rad (Hercules, CA, USA). Sodium phosphate dibasic and monobasic anhydrous were obtained from J. T. Baker (Phillipsburg, NJ, USA), which were used to prepare phosphate solutions at pH 7.0. Milli-Q ultrapure water was used in all experiments.

**Synthesis of PNIPAM MGs.** Surfactant-free emulsion polymerization was applied to prepare PNIPAM MGs.[32] Briefly, 1.13 g (10 mmol) of NIPAM and 80 mg of BIS (cross-linker) were added sequentially to ultrapure water (90 mL) under stirring. The initiator KPS (100 mg) was dissolved in ultrapure water (10 mL). Both solutions were purged with nitrogen for 1 h. After heating the solution of NIPAM and BIS to 70 °C for 30 min, the initiator solution was added to. The mixture reacted at 70 °C under stirring for 4 h. The white mixture was then allowed to cool to ambient temperature (25 °C) under stirring. To purify the PNIPAM MGs, the dispersion was diluted with water (100 mL) and the mixture was then centrifuged at 6511*g* for 50 min. The pellet was redispersed in water and then subjected to three more cycles of centrifugation/wash. The purified PNIPAM MGs were subsequently lyophilized with water (10 mL) for further synthesis.

**Preparation of Au ND−PNIPAM MGs.** Lyophilized PNIPAM MGs (9 mg) in ultrapure water (9.6 mL) was stirred for 5 min and $Au^{3+}$ solution (20 mM, 0.3 mL) was then added to. After stirring the mixture at ambient temperature for 30 min, aqueous NaOH solution (1 M, 0.1 mL) was mixed with THPC solution (80%, 2.45 μL) and then added to the mixture to reduce the $Au^{3+}$ to form small sizes of Au NPs, leading to a color change from colorless to brown over the reaction course of 1 h.[6] The as-prepared Au NPs−NIPAM MGs solution (~10 mL) was then mixed with ultrapure water (7.8 mL), sodium tetraborate (50 mM, pH 9.2, 2 mL), and 11-MUA (1 M, 0.2 mL) in a sample vial (20 mL). The mixture was shaken at ambient temperature for 48 h in the dark. We note that 11-MUA was effective to etch Au NPs to form smaller size of Au NDs under alkaline conditions.[6,33] The mixture was then subjected to four cycles of centrifugation (2650*g*, 20 min)/wash (4 × 10 mL of deionized $H_2O$) to remove the excess 11-MUA. The purified Au ND−NIPAM MGs were then dispersed in ultrapure water (10 mL). For simplicity, its concentration is denoted as "1×".[34] The purified Au ND−PNIPAM MGs were stable for at least 3 months when stored at 4 °C in the dark.

**Characterization.** The absorption and PL spectra of the as-prepared Au ND−PNIPAM MGs solutions were recorded using UV−Vis absorption (GBC, Victoria, Australia) and fluorescence (Cary Eclipse; Varian, CA, USA) spectrophotometers, respectively. Transmission electron microscopy (TEM) and high-resolution TEM (HRTEM) images were recorded using JSM-1200EX II TEM

(JEOL, Ltd., Tokyo, Japan) and FEI Tecnai-G2-F20 TEM systems, respectively. The purified Au ND−PNIPAM MGs were deposited onto a TEM grid with a thin layer of carbon. An energy-dispersive X-ray (EDX) (Philips, Roanoke, VA, U.S.A.) was used to confirm the compositions of Au ND−PNIPAM MGs. A zetasizer (Nano-HT, Malvern, U.K.) was employed to record the dynamic light scattering (DLS) histogram and zeta potentials of Au ND−PNIPAM MGs in various solutions. A Varian 640 Fourier transform infrared (FTIR) spectrophotometer (Varian, CA, USA) was used to analyze the as-prepared PNIPAM and Au ND−PNIPAM MGs. PL images were recorded at ambient temperature on a microscope (BX61; Olympus, Tokyo, Japan) equipped with a 100×/1.40 UPlan-SApo oil objective lens using a digital camera (DP-71; Olympus, Tokyo, Japan). The images were acquired using a DP Controller and a Manager software from Olympus.

**Detection of $Hg^{2+}$.** A stock solution of $Hg^{2+}$ (0.1 M) was prepared in $HNO_3$ (0.1 M, 1 mL), which was further diluted to 0.02−1.0 $\mu$M in ultrapure water. Aliquots of the diluted $Hg^{2+}$ solutions (30 $\mu$L) were separately added to phosphate buffers (5 mM, pH 7.0) containing Au ND−PNIPAM MGs (0.01 X) to give final volumes of 300 $\mu$L. After equilibrating at ambient temperature for 30 min, the mixtures were transferred separately into 96-well microtiter plates and their PL spectra were recorded using a Synergy 4 microplate spectrophometer (BioTek, Winooski, VT, U.S.A.) upon excitation at a wavelength of 375 nm.

**Analysis of Fish Samples.** A selected fish (certified reference material (CRM) dogfish muscle DORM-2) was accurately weighed (0.1 g) and then added to an extraction solution (10 mL) containing HCl (6.0 M) and NaCl (0.1 M). After being subjected to sonication at 55 °C for 45 min, the extracted solution was filtered through a syringe filter (0.45 $\mu$m). Aliquots of $Hg^{2+}$ ion (2 $\mu$M, 0−20 $\mu$L) were spiked into the extracted samples (20 $\mu$L) and ultrapure water were added to give final volumes of 200 $\mu$L. After adding 100% acetonitrile (800 $\mu$L) to the spiked sample, the sample mixtures were equilibrated for 30 min to precipitate proteins. The proteins in the extracted samples were removed through centrifugation (30000*g*, 10 min). The supernatants were then evaporated under vacuum to a final volume of 200 $\mu$L. The deproteinized spiked sample solutions (30 $\mu$L) were then separately added into phosphate solutions (5 mM, pH 7.0) containing Au ND−PNIPAM MGs (0.05×) to give final volumes of 300 $\mu$L. The total concentrations of mercury species in the deproteinized spiked samples were determined through a standard addition method. After equilibrating at ambient temperature for 30 min, the mixtures were transferred separately into 96-well microtiter plates and their PL intensities were then recorded using a microplate spectrophometer. For comparison, the deproteinized spiked samples were also analyzed through ICP-MS.

## RESULTS AND DISCUSSION

**Characterization of the Au ND−PNIPAM MGs.** Figure 1A displays a TEM image of Au ND−PNIPAM MGs having a diameter of 600 ± 21 nm (100 counts), revealing that each MG contained many Au NDs (dark spots). The high-resolution TEM image (Figure 1B) allowed estimation of the size of Au NDs to be 1.8 ± 0.2 nm. The detection of Au in the EDX spectrum (Figure 1C) confirmed the existence of Au NDs in the MGs. We further conducted DLS measurement to determine their hydrodynamic diameters in ultrapure water at 25 °C to be 615 ± 15 nm (see Figure S1 in the Supporting Information). The size estimated from the DLS was only slightly larger than that from the TEM, mainly because the Au ND−PNIPAM MGs were not dehydrated completely prior to TEM measurement.

We further conducted FTIR measurements to determine the compositions of Au ND−PNIPAM MGs, revealing several characteristic peaks at 1550, 1650, 1715, 2970, and 3294 $cm^{-1}$ as displayed in spectrum (a) in Figure 1D. To assign these peaks, FTIR spectra of two controls (PNIPAM and 11-MUA−Au NDs) were recorded separately as displayed in spectra (b) and (c) in Figure 1D. The peaks from PNIPAM were assigned at 1550 $cm^{-1}$ (secondary amide C═O stretching, aka amide II bond), 1650 $cm^{-1}$ (secondary amide C═O stretching, aka amide I bond), 2970 $cm^{-1}$ ($-CH_3$ asymmetric stretching), and 3294 $cm^{-1}$ (secondary amide N−H stretching). On the other hand, the peak at 1715 $cm^{-1}$ (C═O vibrational stretch) was from 11-MUA in the 11-MUA−Au NDs. No peak for the thiol group of 11-MUA in the wavenumber around 2600 $cm^{-1}$ was observed in either spectrum a or c, revealing that 11-MUA molecules were bound to the surfaces of the Au NDs through Au−S bonding.

**Optical Properties and Stability of Au ND−PNIPAM MGs.** Figure 2 displays the absorption and PL spectra of 11-MUA−Au NDs (a) and Au ND−PNIPAM MGs (b), showing their similarity. The maximum absorption wavelength at 375 nm was originated from Au-MUA complexes ($Au^{I}$−thiol complexes) through ligand to metal charge transfer mixed with metal centered (*ds*/*dp*) states modified by Au−Au interaction (LMMCT; S→Au).[35] The emission at 520 nm (excited at 375 nm) of 11-MUA−Au NDs or Au ND−PNIPAM MGs was mainly originated from Au ND/polynuclear gold(I)−thiolate (core/shell) complexes.[36] Slightly broad absorption and PL bands for the Au ND−PNIPAM MGs relative to those for the 11-MUA−Au NDs were mainly due to stronger coupling among the closer Au NDs inside the MGs. A differential refractive index on the surfaces of Au NDs was another contributor. Although the solution colors of Au ND−

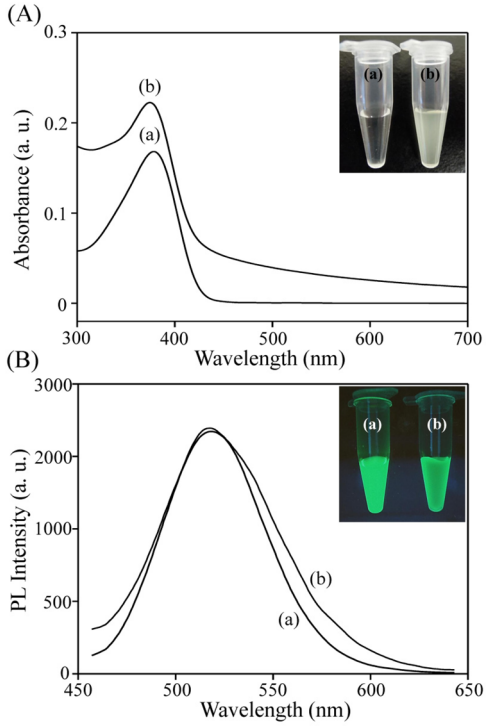


**Figure 2.** (A) UV−vis absorption and (B) PL spectra of (a) 11-MUA−Au NDs and (b) Au ND−PNIPAM MGs. Inset in A: Photographs of (a) 11-MUA−Au NDs and (b) Au ND−PNIPAM MGs solutions without light irradiation. Inset in B: Photographs of (a) 11-MUA−Au NDs and (b) Au ND−PNIPAM MGs solutions upon excitation under a hand-held UV lamp (365 nm). The absorption and PL intensities were plotted in arbitrary units (a.u.).


dx.doi.org/10.1021/am400628p | ACS Appl. Mater. Interfaces 2013, 5, 4383−4388

PNIPAM MGs and 11-MUA–Au NDs were pale yellow and transparent, respectively, they both had green PL color (insets to A and B). Slight differences in the colors were mainly due to the light scattering from the PNIPAM MGs. Like 11-MUA–Au ND, the Au ND–PNIPAM MGs had a large Stokes shift (greater than 130 nm) and QY of 3.8% (quinine as a standard). Unlike the 11-MUA–Au NDs, the Au ND–PNIPAM MGs were purified easily from complicated solution by conducting a centrifugation/wash process. Bright field images of Au ND–PNIPAM MGs and PNIPAM MGs show that the MGs were well-dispersed, whereas their PL images confirm that the PL was from the Au ND–PNIPAM MGs (see Figure S2 in the Supporting Information). We noted that the as-prepared Au ND–PNIPAM MGs were stable for at least three months when stored at 4 °C in the dark.

Figure 3A reveals that the PL intensity of Au ND–PNIPAM MGs (0.01×) reached a maximum at pH 6.0 and gradually

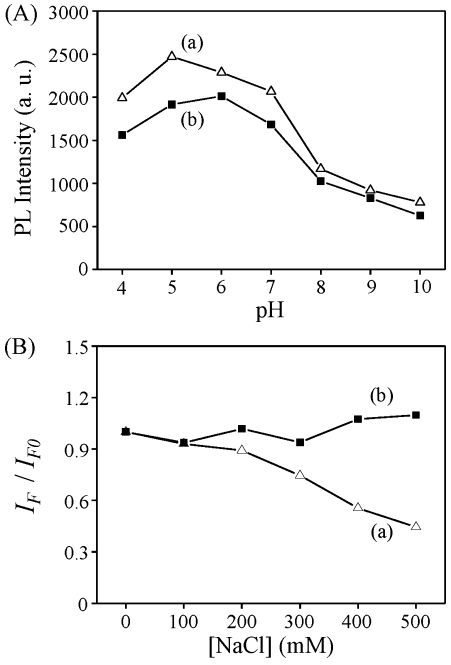


**Figure 3.** Effects of (A) pH (4.0–10.0) and (B) NaCl on (A) PL intensity and (B) relative PL intensity ($I_F/I_{F0}$) of (a) 11-MUA–Au NDs and (b) Au ND–PNIPAM MGs in phosphate solutions. 11-MUA–Au NDs (10 nM) was used as a control (a). Concentrations of Au ND–PNIPAM MGs (b) in A and B were 0.01×. Phosphate solutions: 5 mM in (A), 5 mM (pH 7.0) containing NaCl (0–500 mM) in (B). $I_F$ and $I_{F0}$ represent the PL intensities of the 11-MUA–Au NDs or Au ND–PNIPAM at 520 nm (excitation wavelength: 375 nm) in the presence and absence of NaCl, respectively.

decreased upon increasing the pH values form 6.0 to 10.0, with a trend similar to that of 11-MUA–Au NDs.[37] Upon increasing pH, anionic species such as $OH^-$ and reactive oxygen species increased, leading to greater PL quenching. Figure 3B displays that the Au ND–PNIPAM MGs (0.01 X) were stable in high-salt media; only a 9% increase in the PL in the presence of 500 mM NaCl was observed. Upon increasing NaCl concentration, decreases in the PNIPAM–$H_2O$ hydrogen bonds led to deswelling of the MGs.[38,39] The PL intensities of Au ND–PNIPAM MGs at different concentrations of NaCl were almost the same, revealing that PNIPAM MGs protected Au NDs from salt-induced PL quenching. As a control, we also investigated the stability of 11-MUA–Au NDs (10 nM) in the presence of NaCl; about 55% PL quenching occurred in the presence of 500 mM NaCl. The results revealed that the PNIPAM MGs minimized the access of NaCl to the surface of Au NDs.

We separately investigated the morphology and color of 11-MUA–Au NDs and Au ND–PNIPAM MG solutions under heating–cooling cycles in the temperature range 20–50 °C. PNIPAM is a thermoresponsive polymer that undergoes a coil-to-globule transition in aqueous media at 32 °C.[40] Figure S3A in the Supporting Information shows the turbidity of Au ND–PNIPAM MGs solution increased upon increasing the temperature from 20 to 50 °C, which was restored by cooling the temperature back to 20 °C. The swelling–deswelling behavior of Au ND–PNIPAM MGs was related to the hydrogen bonding between PNIPAM chains and water, which was disrupted upon heating, leading to collapse of their gradual chain.[41] The PL spectra of 11-MUA–Au NDs and Au ND–PNIPAM MGs were investigated at various temperatures. Figure S3B in the Supporting Information reveals the PL intensities of 11-MUA–Au NDs were almost constant in the temperatures range over 25 to 52 °C. However, when the temperature was increased to that around the lower critical solution temperature (32 °C) of PNIPAM, the PL intensities of Au ND–PNIPAM MGs decreased sharply (see Figure S3C in the Supporting Information) as a result of aggregation of the Au NDs. At a temperature above the LCST of PNIPAM MGs, the trapping of Au NDs by the gel became weaker as a result of decreases in the hydrogen bonding between the carboxyl groups of 11-MUA capped on the Au NDs and the amide group on the PNIPAM.[29,42]

**Detection of $Hg^{2+}$ Ions Using Au ND–PNIPAM MGs.** Figure 4A displays the PL of Au ND–PNIPAM MGs (0.01×) decreased upon increasing $Hg^{2+}$ concentration in phosphate solution (5 mM, pH 7.0). We noted that $Hg^{2+}$ induced negligible changes in the absorbance at 375 nm. The value of $(I_{F0} - I_F)/I_{F0}$ versus the concentrations of $Hg^{2+}$ decreased linearly ($r = 0.9945$) upon increasing the concentration of $Hg^{2+}$ over the range 2–20 nM (inset to Figure 4A), in which $I_{F0}$ and $I_F$ are the PL of Au ND–PNIPAM MGs in the absence and presence of $Hg^{2+}$, respectively. This approach provided a limit of detection (LOD) at signal-to-noise ratio of 3 to be 1.7 nM for $Hg^{2+}$ ions, which was comparable to that provided by 11-MUA–Au NDs.[6] The LOD of Au ND–PNIPAM MGs for $Hg^{2+}$ in phosphate solution (5 mM, pH 7.0) containing 500 mM NaCl was 1.9 nM, showing a negligible effect of salt on the detection of $Hg^{2+}$ when using Au ND–PNIPAM MGs probe. However, 11-MUA–Au NDs did not allow quantitative detection of $Hg^{2+}$ in the same condition. The selectivity of the Au ND–PNIPAM MG probe (0.01×) toward $Hg^{2+}$ (10 nM) against one of the following ions: $Cu^{2+}$, $Na^+$, $Ca^{2+}$, $Mn^{2+}$, $Zn^{2+}$, $Fe^{3+}$, $Mg^{2+}$, $K^+$, $Cd^{2+}$, $Pb^{2+}$, $Ni^{2+}$, $Cr^{2+}$, $Fe^{2+}$ (each 100 nM) were investigated. Figure 4B reveals that the probe responded selectively toward $Hg^{2+}$ over the other tested metal ions. We further conducted the Au ND–PNIPAM MGs probe (0.01×) to detect $Hg^{2+}$ in the presence of the other interfering metal ions (see Figure S4 in the Supporting Information). The tolerance concentrations of other metal ions (within a relative error of ±5%) when applying the Au ND–PNIPAM MGs probe for the detection of $Hg^{2+}$ ions (10 nM) were at least 100 nM.

To understand the quenching mechanism, the zeta potentials of the Au ND–PNIPAM MGs (0.5 X) in the presence of $Hg^{2+}$ at various concentrations were recorded. Figure S5A in the

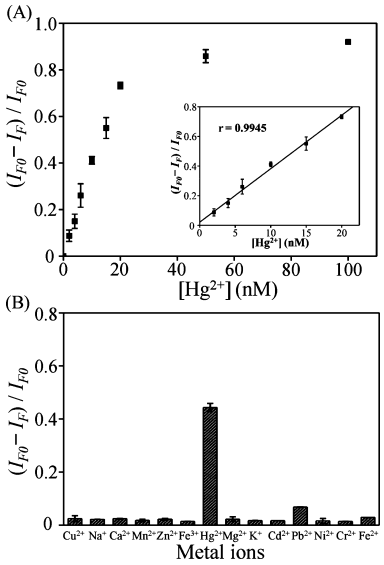


**Figure 4.** (A) Sensitivity and (B) selectivity of the Au ND−PNIPAM MGs for $Hg^{2+}$. (A) Relative PL intensity $[(I_{F0}-I_F)/I_{F0}]$ at 520 nm of the Au ND−PNIPAM MGs (0.01×) in the presence of $Hg^{2+}$ ions (0−100 nM) in phosphate solution (5 mM, pH 7.0). Inset: Linearity of the probe for $Hg^{2+}$ over the concentration range 2−20.0 nM. Relative standard deviations (RSD) of $Hg^{2+}$ at 10, 20, and 50 nM were 3.9, 1.8, and 3.2% ($n$ = 3), respectively. (B) Plots of PL spectra of relative PL intensity $[(I_{F0}-I_F)/I_{F0}]$ of Au ND−PNIPAM MGs (0.01X) in the presence of $Hg^{2+}$ ions (10 nM) and various metal ions (100 nM) in phosphate solutions (5 mM, pH 7.0). The incubation time was 30 min. Error bars represent standard deviations from three replicate measurements.

Supporting Information shows that the zeta potential of Au ND−PNIPAM MGs shifted to less negative values; it changed from −42.6 to −11.1 mV upon increasing $Hg^{2+}$ concentration from 0 to 50 $\mu$M, indicating deposition of $Hg^{2+}$ ions onto the surfaces of the Au NDs inside the Au ND−PNIPAM MGs. It is well-known that $Hg^{2+}$ easily forms Au−Hg amalgam on Au NP surfaces.[43−48] In addition, $Hg^{2+}$ formed complexes with MUA on the surfaces of Au NDs, bringing the Au NDs closer inside the MGs (self-quenching). To further support our reasoning, we recorded the static light scattering intensities of the solutions, showing the intensity gradually increased from 159.5 to 272.1 kcps when $Hg^{2+}$ concentration was raised from 0 to 50 $\mu$M. PL microscopy and TEM images confirmed the aggregation of Au ND−PNIPAM MGs in the presence of $Hg^{2+}$ (see Figure S5B in the Supporting Information). The ICP-MS data revealed that a higher amount of $Hg^{2+}$ ions was observed in the Au ND−PNIPAM MGs than in the bare PNIPAM MGs (0.622 $\mu$g $Hg^{2+}$/mg PNIPAM MGs vs 0.064 $\mu$g $Hg^{2+}$/mg PNIPAM MGs). PL quenching of Au NDs due to the formation of Au−Hg amalgam has been demonstrated.[6,7,9−11] In addition, self PL quenching due to the formation of Au ND−PNIPAM MGs aggregates could not be ruled out.

**Detection of $Hg^{2+}$ in Fish Samples.** Practicality of the Au ND−PNIPAM MGs probe was validated for the determination of the concentration of $Hg^{2+}$ in fish samples. By applying a standard addition, the concentration of $Hg^{2+}$ in a representative diluted sample from three repeated measurements was determined to be 2.20 (±0.18) nM. By counting the dilution factor, we calculated the concentration of total Hg species in the fish sample to be 4.45 (±0.76) mg $kg^{-1}$ (cf. values of 4.64 (±0.26) mg $kg^{-1}$ provided by NRC). Using a student $t$ test, the 95% confidence interval for total Hg species was found to be 4.38−4.90 mg $kg^{-1}$, revealing that no significant differences existed between the values measured using our approach and the true values.

## CONCLUSIONS

Unlike Au NDs that could only be purified by conducting dialysis or gel separation, the as-prepared Au ND−PNIPAM MGs could be easily and rapidly purified by conducting centrifugation. Because $Hg^{2+}$ caused the formation of Au−Hg amalgam and Au ND−PNIPAM MG aggregates that led to decreased PL of the Au ND−PNIPAM MGs, this present probe allowed sensitive and selective detection of $Hg^{2+}$. The Au ND−PNIPAM MGs exhibited great stability against salt, which allowed detection of $Hg^{2+}$ at the concentration down to 1.9 nM in aqueous solution containing 500 mM NaCl. Our study results clearly showed that the Au ND−PNIPAM MG probe holds great potential for the determination of the concentrations of $Hg^{2+}$ ions in the environmental and biological samples.

## ASSOCIATED CONTENT

### Supporting Information

Figures S1−S5 provide some properties of Au ND−PNIPAM MGs, like particle size, PL images, thermoresponsive behavior, and the photoluminescent quenching mechanism of Au ND−PNIPAM MGs by $Hg^{2+}$. This material is available free of charge via the Internet at http://pubs.acs.org.

## AUTHOR INFORMATION

### Corresponding Author

***Corresponding Author** E-mail: changht@ntu.edu.tw.

### Notes

The authors declare no competing financial interest.

## ACKNOWLEDGMENTS

This study was supported by the National Science Council of Taiwan under contract NSC 101-2113-M-002-002-MY3.

## REFERENCES

(1) Wang, Q.; Kim, D.; Dionysiou, D. D.; Sorial, G. A.; Timberlake, D. *Environ. Pollut.* **2004**, *131*, 323−336.
(2) Tan, Z.-Q.; Liu, J.-F.; Liu, R.; Yin, Y.-G.; Jiang, G.-B. *Chem. Commun.* **2009**, 7030−7032.
(3) Huang, C.-C.; Chang, H.-T. *Chem. Commun.* **2007**, 1215−1217.
(4) Darbha, G. K.; Singh, A. K.; Rai, U. S.; Yu, E.; Yu, H.; Ray, P. C. *J. Am. Chem. Soc.* **2008**, *130*, 8038−8043.
(5) Huang, C.-C.; Chang, H.-T. *Anal. Chem.* **2006**, *78*, 8332−8338.
(6) Huang, C.-C.; Yang, Z.; Lee, K.-H.; Chang, H.-T. *Angew. Chem., Int. Ed.* **2007**, *46*, 6824−6828.
(7) Wei, H.; Wang, Z.; Yang, L.; Tian, S.; Hou, C.; Lu, Y. *Analyst* **2010**, *135*, 1406−1410.
(8) Lin, Y.-H.; Tseng, W.-L. *Anal. Chem.* **2010**, *82*, 9194−9200.
(9) Xie, J.; Zheng, Y.; Ying, J. Y. *Chem. Commun.* **2010**, *46*, 961−963.
(10) Chen, P.-C.; Chiang, C.-K.; Chang, H.-T. *J. Nanopart. Res.* **2013**, *15*, 1336.
(11) Kawasaki, H.; Hamaguchi, K.; Osaka, I.; Arakawa, R. *Adv. Funct. Mater.* **2011**, *21*, 3508−3515.
(12) Muhammed, M. A. H.; Verma, P. K.; Pal, S. K.; Retnakumari, A.; Koyakutty, M.; Nair, S.; Pradeep, T. *Chem.—Eur. J.* **2010**, *16*, 10103−10112.
(13) Shang, L.; Yang, L.; Stockmar, F.; Popescu, R.; Trouillet, V.; Bruns, M.; Gerthsen, D.; Nienhaus, G. U. *Nanoscale* **2012**, *4*, 4155−4160.

(14) Guo, W.; Yuan, J.; Wang, E. *Chem. Commun.* **2009**, 3395−3397.
(15) Adhikari, B.; Banerjee, A. *Chem. Mater.* **2010**, *22*, 4364−4371.
(16) Guo, C.; Irudayaraj, J. *Anal. Chem.* **2011**, *83*, 2883−2889.
(17) Xue, X.; Wang, F.; Liu, X. *J. Am. Chem. Soc.* **2008**, *130*, 3244−3245.
(18) Liu, C.-W.; Hsieh, Y.-T.; Huang, C.-C.; Lin, Z.-H.; Chang, H.-T. *Chem. Commun.* **2008**, 2242−2244.
(19) Wang, L.; Li, T.; Du, Y.; Chen, C.; Li, B.; Zhou, M.; Dong, S. *Biosens. Bioelectron.* **2010**, *25*, 2622−2626.
(20) Liu, C.-W.; Huang, C.-C.; Chang, H.-T. *Anal. Chem.* **2009**, *81*, 2383−2387.
(21) Lin, Y.-W.; Chang, H.-T. *Analyst* **2011**, *136*, 3323−3328.
(22) Zhu, Z.; Su, Y.; Li, J.; Li, D.; Zhang, J.; Song, S.; Zhao, Y.; Li, G.; Fan, C. *Anal. Chem.* **2009**, *81*, 7660−7666.
(23) Kong, R.-M.; Zhang, X.-B.; Zhang, L.-L.; Jin, X.-Y.; Huan, S.-Y.; Shen, G.-L.; Yu, R.-Q. *Chem. Commun.* **2009**, 5633−5635.
(24) Kim, H.-N.; Lee, M.-H.; Kim, H.-J.; Kim, J.-S.; Yoon, J. *Chem. Soc. Rev.* **2008**, *37*, 1465−1472.
(25) Shi, L.; Song, W.; Li, Y.; Li, D.-W.; Swanick, K. N.; Ding, Z.; Long, Y.-T. *Talanta* **2011**, *84*, 900−904.
(26) Shi, L.; Li, Y.; Liu, Z.-P.; James, T. D.; Long, Y.-T. *Talanta* **2012**, *100*, 401−404.
(27) Chen, J.; Liu, M.; Chen, C.; Gong, H.; Gao, C. *ACS Appl. Mater. Interfaces* **2011**, *3*, 3215−3223.
(28) Karg, M.; Hellweg, T. *Curr. Opin. Colloid Interface Sci.* **2009**, *14*, 438−450.
(29) Wang, Y.-Q.; Zhang, Y.-Y.; Zhang, F.; Li, W.-Y. *J. Mater. Chem.* **2011**, *21*, 6556−6562.
(30) Xu, S.; Zhang, J.; Paquet, C.; Lin, Y.; Kumacheva, E. *Adv. Funct. Mater.* **2003**, *13*, 468−472.
(31) Fernández-López, C.; Pérez-Balado, C.; Pérez-Juste, J.; Pastoriza-Santos, I.; R. de Lera, Á.; Liz-Marzán, L. M. *Soft Matter.* **2012**, *8*, 4165−4170.
(32) Pelton, R. H.; Chibante, P. *Colloids Surf.* **1986**, *20*, 247−256.
(33) Huang, C.-C.; Liao, H.-Y.; Shiang, Y.-C.; Lin, Z.-H.; Yang, Z.; Chang, H.-T. *J. Mater. Chem.* **2009**, *19*, 755−759.
(34) Huang, C.-C.; Chen, C.-T.; Shiang, Y.-C.; Lin, Z.-H.; Chang, H.-T. *Anal. Chem.* **2009**, *81*, 875−882.
(35) Volger, A.; Kunkely, H. *Coord. Chem. Rev.* **2001**, *219*, 489−507.
(36) Parker, J. F.; Fields-Zinna, C. A.; Murray, R. W. *Acc. Chem. Res.* **2010**, *43*, 1289−1296.
(37) Shiang, Y.-C.; Huang, C.-C.; Chang, H.-T. *Chem. Commun.* **2009**, 3437−3439.
(38) López-León, T.; Elaïssari, A.; Qrtega-Vinuesa, J. L.; Bastos-González, D. *Chem. Phys. Chem* **2008**, *8*, 148−156.
(39) López-León, T.; Qrtega-Vinuesa, J. L.; Bastos-González, D.; Elaïssari, A. *J. Phys. Chem. B* **2006**, *110*, 4629−4636.
(40) Saunders, B. R.; Vincent, B. *Adv. Colloid Interface Sci.* **1999**, *80*, 1−25.
(41) Lyon, L. A.; Meng, Z.; Singh, N.; Sorrell, C. D.; John, A. St. *Chem. Soc. Rev.* **2009**, *38*, 865−874.
(42) Gong, Y.; Gao, M.; Wang, D.; Möhwald, H. *Chem. Mater.* **2005**, *17*, 2648−2653.
(43) Zierhut, A.; Leopold, K.; Harwardt, L.; Worsfold, P.; Schuster, M. *J. Anal. At. Spectrom.* **2009**, *24*, 767−774.
(44) Mertens, S. F. L.; Gara, M.; Sologubenko, A. S.; Mayer, J.; Szidat, S.; Krämer, K. W.; Jacob, T.; Schiffrin, D. J.; Wandlowski, T. *Adv. Funct. Mater.* **2011**, *21*, 3259−3267.
(45) Zaleski-Ejgierd, P.; Pyykkö, P. *J. Phys. Chem. A* **2009**, *113*, 12380−12385.
(46) Henglein, A.; Giersig, M. *J. Phys. Chem. B* **2000**, *104*, 5056−5060.
(47) Rex, M.; Hernandez, F. E.; Campiglia, A. D. *Anal. Chem.* **2006**, *78*, 445−451.
(48) Wang, C.-I.; Huang, C.-C.; Lin, Y.-W.; Chen, W.-T.; Chang, H.-T. *Anal. Chim. Acta* **2012**, *745*, 124−130.